

Half-Sandwich Cyclopentadienylruthenium(II) Complexes: A New Antimalarial Chemotype

Sofia A. Milheiro, Joana Gonçalves, Ricardo M. R. M. Lopes, Margarida Madureira, Lis Lobo, Andreia Lopes, Fátima Nogueira, Diana Fontinha, Miguel Prudêncio, M. Fátima M. Piedade, Sandra N. Pinto, Pedro R. Florindo,* and Rui Moreira



Cite This: <https://dx.doi.org/10.1021/acs.inorgchem.0c01795>



Read Online

ACCESS |



Metrics & More

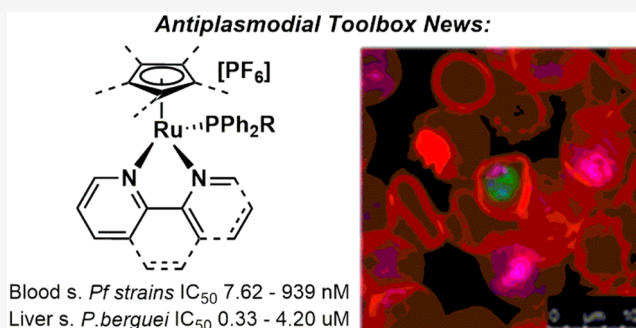


Article Recommendations



Supporting Information

ABSTRACT: A small library of “half-sandwich” cyclopentadienylruthenium(II) compounds of the general formula $[(\eta^5\text{-C}_5\text{R}_5)\text{Ru}(\text{PPh}_3)(\text{N-N})][\text{PF}_6]$, a scaffold hitherto absent from the toolbox of antiplasmodials, was screened for activity against the blood stage of CQ-sensitive 3D7-GFP, CQ-resistant Dd2, and artemisinin-resistant IPC5202 *Plasmodium falciparum* strains and the liver stage of *Plasmodium berghei*. The best-performing compounds displayed dual-stage activity, with single-digit nanomolar IC_{50} values against blood-stage malaria parasites, nanomolar activity against liver-stage parasites, and residual cytotoxicity against HepG2 and Huh7 mammalian cells. The parasitic absorption/distribution of 7-nitrobenzoxadiazole-appended fluorescent compounds **Ru4** and **Ru5** was investigated by confocal fluorescence microscopy, revealing parasite-selective absorption in infected erythrocytes and nuclear accumulation of both compounds. The lead compound **Ru2** impaired asexual parasite differentiation, exhibiting fast parasitocidal activity against both ring and trophozoite stages of a synchronized culture of the *P. falciparum* 3D7 strain. These results point to cyclopentadienylruthenium(II) complexes as a highly promising chemotype for the development of dual-stage antiplasmodials.



INTRODUCTION

Malaria is a public health concern of tragic proportions, with an estimated 228 million new cases and 405000 deaths globally in 2018, 67% of whom were children under 5 years of age.¹ This disease is caused by parasites of the genus *Plasmodium* that, upon injection in a mammalian host through the bite of an infected *Anopheles* mosquito, travel to the liver, initiating the hepatic stage of infection. This culminates in the release of blood-infectious parasites that lead to the blood stage of infection and the clinical symptoms that are associated with malaria. Very few drugs tackle the asymptomatic but obligatory liver-stage bottleneck of infection, creating a gap in effective prophylactic measures against malaria.² Furthermore, the effectiveness of available antiplasmodial drugs against the blood stage of infection is increasingly threatened by the emergence and spread of drug-resistant parasites. Chloroquine [CQ (Figure 1)], the cornerstone antiplasmodial drug for many decades, is now largely ineffective against *Plasmodium falciparum* (*Pf*), the deadliest malaria parasite, due to widespread resistance to this drug.^{3,4} Currently, artemisinin-based combination therapies (ACTs), in which artemisinin or its derivatives (artesunate, artemether, and dihydroartemisinin) are combined with longer-acting antiplasmodial drugs with distinct modes of action to prevent resistance development, are

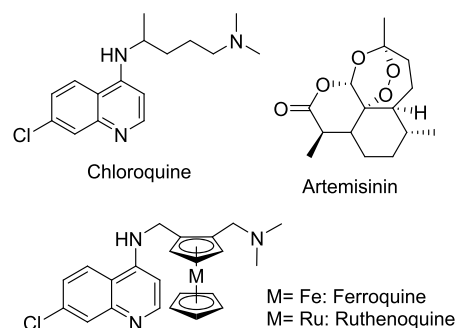


Figure 1. Antimalarials chloroquine, artemisinin, and chloroquine–metalocene hybrids ferroquine and ruthenoquine.

the front-line malaria therapeutics, with treatment success rates of >95%.¹ Nonetheless, resistance to ACTs appears to be

Received: June 17, 2020

emerging in some regions of the world, as *PfKelch13* mutations, associated with artemisinin resistance, are widespread in Southeast Asian countries and have also been detected in some African countries.^{1,3,4} Thus, the discovery of new antiparasmodial drugs that tackle both stages of *Plasmodium* infection in the mammalian host remains an urgent clinical need.

Metal complexes are especially attractive for drug design, as they offer structural and physicochemical possibilities that cannot be attained by organic molecules.⁵ The clinical success of platinum anticancer drugs⁶ and of the antirheumatic agent auranofin⁷ has inspired bioinorganic/organometallic drug development over the past several decades, leading to promising lead drugs against cancer and other diseases.^{8–14} In malaria, ferroquine [FQ (Figure 1)], an organometallic ferrocenyl–chloroquine hybrid molecule, is active against both CQ-sensitive and CQ-resistant *P. falciparum* strains *in vitro* and CQ-resistant *Plasmodium vinckei vinckei* strains *in vivo* and is currently undergoing phase IIb clinical trials in combination with artefenomel, a trioxalane.¹⁵ The success of FQ led to intense research of metal-based antiparasmodial drugs, mostly focused on ferrocenyl and other metallic hybrids with CQ or artemisinin derivatives.^{16–18}

Prompted by the early success of ruthenium(III) compounds NAMI-A $\{(\text{ImH})[\text{trans-RuCl}_4(\text{dmsO-S})(\text{Im})]\}$, where Im = imidazole} and KP1019/1339 $\{\text{KP1019} = (\text{IndH})[\text{trans-RuCl}_4(\text{Ind})_2]\}$, where Ind = indazole and KP1339 = $\text{Na}[\text{trans-RuCl}_4(\text{Ind})_2]\}$, which entered clinical trials as antimetastatic and cytotoxic agents, respectively, ruthenium(II) compounds emerged as the most studied and promising among non-platinum chemotherapeutic alternatives.^{19–21} Compounds $[(\eta^6\text{-C}_6\text{H}_5\text{C}_6\text{H}_5)\text{RuCl}(\text{H}_2\text{NCH}_2\text{CH}_2\text{NH}_2\text{-N,N}')][\text{PF}_6]$ (RM175),^{22,23} $[(\eta^6\text{-C}_6\text{H}_5\text{Me})\text{RuCl}_2(\text{PTA})]$ [PTA = 1,3,5-triaza-7-phosphadamantane (RAPTA-T)],^{24,25} and $[\text{Ru}(\text{Phen})(\kappa\text{-C,N-(2-phenyl-pyridine)})(\text{NCMe})_2][\text{PF}_6]$ (RDC11)^{26,27} entered preclinical evaluation as anticancer (RM175 and RDC11) and antimetastatic agents (RAPTA-T), and recently, compound $[\text{Ru}(\text{dmb})_2(\text{IP-TT})]\text{Cl}_2$ [dmb = 4,4'-dimethyl-2,2'-bipyridine; IP-TT = 2-(2',2'':5'',2''-terthiophene)-imidazol[4,5-f][1,10]phenanthroline] (TLD1433) entered a phase II clinical trial as a cancer photodynamic therapy photosensitizer (PDT PS) for the treatment of non-muscle invasive bladder cancer (Figure 2).²⁸

In the field of malaria chemotherapy, ruthenium was employed as ruthenoquine (Figure 1), a ruthenium analogue

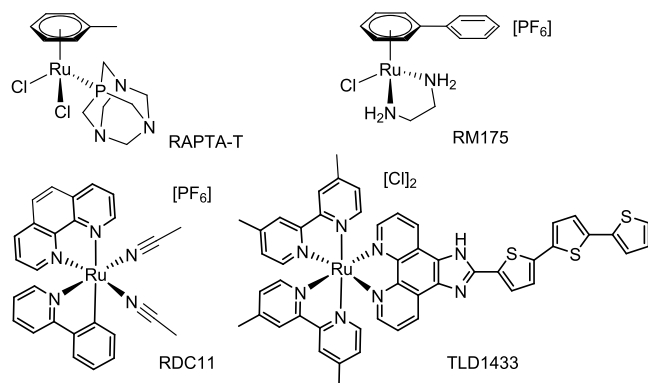


Figure 2. Anticancer ruthenium(II) compounds RAPTA-T,^{24,25} RM175,^{22,23} and RDC11^{26,27} and PDT photosensitizer TLD1433.²⁸

of FQ, displaying *in vitro*, but not *in vivo*, antiparasmodial activity.²⁹ Ruthenium(II) arene compounds were also reported as antiparasmodials, in combination with chloroquine or other active antiparasmodial scaffolds (Figure 3), displaying *in vitro*^{30–38} and *in vivo*³⁹ antiparasmodial activity.

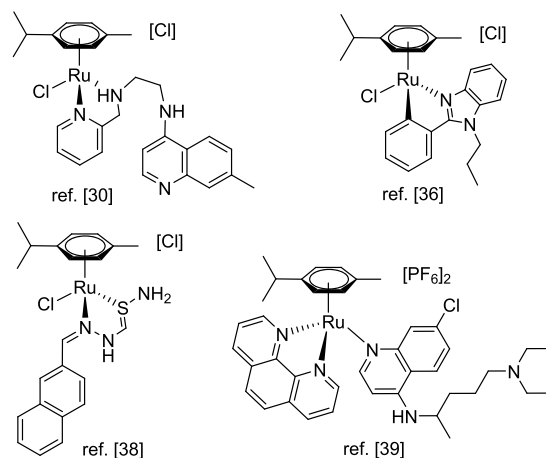


Figure 3. Ruthenium(II)-arene compounds with antiparasitic activity (*P. falciparum*).

The design of metal-based antiparasmodial drugs has been driven by the hypothesis that conjugation of organic ligand scaffolds with pharmacological activity with an (organo)-metallic moiety can lead to new drugs with improved pharmacological profile, which act on multiple targets. In contrast, attempts to uncover new metal-based antiparasmodial lead scaffolds are scarce. Challenging the “mainstream” design rationale, we decided to assess the antiparasmodial activity of five half-sandwich cyclopentadienylruthenium(II) complexes of the general formula $[(\eta^5\text{-C}_5\text{R}_5)\text{Ru}(\text{PPh}_3)(\text{N-N})][\text{PF}_6]$, a scaffold previously featured in anticancer studies,^{40–43} but hitherto absent from the toolbox of antiparasmodial compounds. To gain visual insight into the parasitic/cellular distribution of organometallic complexes, we developed two 7-nitrobenzoxadiazole (NBD)-appended fluorescent compounds.

EXPERIMENTAL SECTION

Chemistry. General Procedures. Reagents were bought from commercial sources and used without further purification. Compounds Ru1 and Ru2 were previously reported^{40–42} but were obtained for this study using a different synthetic methodology. Reaction/crystallization solvents were dried according to standard procedures.⁴⁴ ¹H nuclear magnetic resonance (NMR) spectra were recorded on a Bruker Ultra-Shield 300 MHz spectrometer operating at 300 MHz, at probe temperature. Chemical shifts are quoted on the δ scale, in parts per million, using residual solvent peaks as the internal standard. Coupling constants (*J*) are reported in hertz with the following splitting abbreviations: s, singlet; br., broad; d, doublet; t, triplet; q, quartet; p, quintet; m, multiplet. Thin layer chromatography (TLC) was carried out using Merck aluminum-backed sheets coated with 60 F254 silica gel. Flash column chromatography was performed using Merck 60 (230–400 mesh ASTM) silica gel. Ultraviolet (UV) spectra were traced in a Thermo Scientific Evolution 201 UV–visible spectrophotometer. Fluorescence measurements were taken on a SHIMADZU spectrofluorophotometer RF-6000 instrument. LC-MS analysis was performed in an HPLC Dionex Ultimate 3000 instrument composed of a model HPG3200 binary pump, a model WPS300 autosampler, and a model TCC3000 column oven coupled in-line to a LCQ Fleet ion trap mass spectrometer equipped with an ESI ion source (Thermo Scientific). Aliquots of 10 μL were injected

into the column via a Rheodyne injector with a 25 μL loop, in the partial injection mode. Separations were carried out with a Luna C18 100 Å column (150 mm \times 2 mm, 5 μm) at 30 $^{\circ}\text{C}$, using a flow rate of 0.2 mL min^{-1} , a mobile phase of 0.1% acid formic in water (v/v, eluent A) and acetonitrile (eluent B), and a 30 min linear gradient from 5% A to 70% B, followed by a 2 min a linear gradient to 100% B, followed by a 8 min isocratic gradient to 100% B, and then the column was re-equilibrated with 5% B for 10 min. The mass spectrometer was operated in the ESI positive and negative ion modes, with the following optimized parameters: ion spray voltage, ± 4.5 kV; capillary voltage, 16/−18 V; tube lens offset, −70/58 V; sheath gas (N_2), 40 arbitrary units; auxiliary gas (N_2), 20 arbitrary units; capillary temperature, 300 $^{\circ}\text{C}$. Spectra typically correspond to the average of 20–35 scans and were recorded between 100 and 850 Da. C/H/N elemental analysis was determined using a FLASH 2000 Series CHNS/O Analyzer (Thermo Scientific) equipped with a thermal conductivity detector. Eager Xperience software was used for data acquisition and processing.

Synthesis and Characterization. Compound 1. 4-Chloro-7-nitrobenzo[*c*][1,2,5]oxadiazole (400 mg, 2 mmol) was added to a solution of 3-azidopropan-1-amine (203 mg, 2 mmol) in methanol (10 mL). After the mixture had been stirred for 30 min at room temperature, the solvent was evaporated under reduced pressure. The crude product was purified by flash chromatography (1:1 AcOEt/*n*-hexane eluent), affording *N*-(3-azidopropyl)-7-nitrobenzo[*c*][1,2,5]-oxadiazol-4-amine (195 mg, 0.75 mmol, $\eta = 37\%$). The product was dissolved in THF (5 mL) and CuI (141 mg, 0.75 mmol); 2-ethynylpyridine (114 μL , 1.1 mmol) and DIPEA (260 μL , 1.5 mmol) were added, and the mixture was stirred at 80 $^{\circ}\text{C}$ for 2 h. The solvent was then removed under reduced pressure, and the crude product was purified by flash chromatography (eluent of 0–5% MeOH in AcOEt), affording 7-nitro-*N*-{3-[4-(pyridin-2-yl)-1*H*-1,2,3-triazol-1-yl]propyl}-benzo[*c*][1,2,5]oxadiazol-4-amine (**1**) as an orange solid (178 mg, $\eta = 65\%$). $^1\text{H NMR}$ (300 MHz, DMSO): δ 9.47 (br. s, 1H, H2), 8.67 (s, 1H, H8), 8.58 (br. s, 1H, H5), 8.49 (d, 1H, $J = 8.9$ Hz, H6'), 7.99 (br. s, 1H, H4), 7.89 (t, 1H, $J = 7.2$ Hz, NH), 7.33 (br. s, 1H, H3), 6.40 (d, $J = 9.0$ Hz, 1H, H5'), 4.58 (t, $J = 6.7$ Hz, 2H, H10), 3.55 (br. s, 2H, H12), 2.41–2.26 (m, 2H, H11). MS [ESI]: m/z [M + H] $^+$ calcd for $\text{C}_{16}\text{H}_{14}\text{N}_8\text{O}_3$, 367.12, found 367.13. Anal. Calcd for $\text{C}_{16}\text{H}_{14}\text{N}_8\text{O}_3$: C, 52.46; H, 3.85; N, 30.59. Found: C, 52.87; H, 4.07; N, 28.83.

Compound 2. 4-Chloro-7-nitrobenzo[*c*][1,2,5]oxadiazole (400 mg, 2 mmol) was added to a solution of *tert*-butyl (3-aminopropyl)-carbamate (348 mg, 2 mmol) in methanol (10 mL), and the mixture was stirred for 30 min at room temperature. The solvent was removed under reduced pressure. The crude product was dissolved in CH_2Cl_2 (3 mL); trifluoroacetic acid (2 mL) was added, and the mixture was stirred at room temperature for 20 min. The volatiles were evaporated under reduced pressure, and the crude product was purified by flash chromatography (eluent of 0–5% MeOH in AcOEt), affording *N* 1 -(7-nitrobenzo[*c*][1,2,5]oxadiazol-4-yl)propane-1,3-diamine (91 mg, 0.38 mmol, $\eta = 19\%$). The product was dissolved in DMF (2 mL) and added to a solution of TBTU (134 mg, 0.42 mmol), DIPEA (139 μL , 0.8 mmol), and 4-diphenylphosphine benzoic acid (260 μL , 1.5 mmol) in DMF (5 mL), and the mixture was stirred overnight at room temperature. The volatiles were then removed under reduced pressure, and the crude product was purified by flash chromatography (AcOEt eluent), affording 4-(diphenylphosphanyl)-*N*-{3-[(7-nitrobenzo[*c*][1,2,5]oxadiazol-4-yl)amino]propyl} benzamide as a yellow solid (147 mg, $\eta = 74\%$). $^1\text{H NMR}$ (300 MHz, DMSO): δ 9.48 (s, 1H, NHCO), 8.56–8.48 (complex, 2H, H6' + NH), 7.81 (d, 2H, $J = 7.1$ Hz, H2), 7.48–7.35 (m, 6H, PPh₂), 7.34–7.18 (complex, 6H, PPh₂ + H3), 6.42 (d, $J = 9.0$ Hz, 1H, H5'), 3.55 (s, 2H, H9), 3.39 (m, 2H, H7), 2.03–1.87 (m, 2H, H8). MS [ESI]: m/z [M + H] $^+$ calcd for $\text{C}_{28}\text{H}_{24}\text{N}_5\text{O}_4\text{P}$, 542.15, found 542.25. Anal. Calcd for $\text{C}_{28}\text{H}_{24}\text{N}_5\text{O}_4\text{P}$: C, 64.00; H, 4.60; N, 13.33. Found: C, 63.81; H, 4.82; N, 13.20.

Synthesis of Ru1, Ru2, Ru4, and Ru5. CH_2Cl_2 (15 mL) was added to a Schlenk tube charged with $[(\eta^5\text{-C}_5\text{H}_5)\text{Ru}(\text{NCCH}_3)]_2[\text{PF}_6]_2$ (0.20 mmol), phosphine (0.21 mmol; **Ru1**, **Ru2**, and **Ru4**, PPh₃; **Ru5**, compound **2**), and the *N*-*N* bidentate ligand (0.21 mmol; **Ru1** and

Ru5, 2,2'-bipyridyl; **Ru2**, 1,10-phenanthroline; **Ru4**, compound **1**), and the mixture was stirred overnight at room temperature. The solutions were then filtered via canula and pumped to dryness. Crude products were washed with *n*-hexane (10 mL) and ethyl ether (10 mL) and recrystallized by slow diffusion of *n*-hexane in acetone or dichloromethane solutions.

Ru1, $[(\eta^5\text{-C}_5\text{H}_5)\text{Ru}(2,2'\text{-bipyridyl})(\text{PPh}_3)]_2[\text{PF}_6]_2$. $\eta = 82\%$. Orange. $^1\text{H NMR}$ (300 MHz, DMSO): δ 9.36 (d, 2H, $J = 5.5$ Hz, H2), 8.17 (d, 2H, $J = 8.1$ Hz, H5), 7.84 (t, 2H, $J = 7.8$ Hz, H4), 7.44–7.35 (m, 3H, PPh₃), 7.35–7.24 (complex, 8H, H3 + PPh₃), 6.95 (m, 6H, PPh₃), 4.86 (s, 5H, $\eta^5\text{-C}_5\text{H}_5$). Anal. Calcd for $\text{C}_{33}\text{H}_{28}\text{F}_6\text{N}_2\text{P}_2\text{Ru}$: C, 54.33; H, 3.82; N, 3.84. Found: C, 54.16; H, 3.76; N, 3.61.

Ru2, $[(\eta^5\text{-C}_5\text{H}_5)\text{Ru}(1,10\text{-phenanthroline})(\text{PPh}_3)]_2[\text{PF}_6]_2$. $\eta = 87\%$. Red. $^1\text{H NMR}$ (300 MHz, DMSO): δ 9.73 (d, 2H, $J = 5.3$ Hz, H2), 8.45 (d, 2H, $J = 8.1$ Hz, H4), 7.96 (s, 2H, H6), 7.73 (dd, 2H, $J = 8.1$, 5.3 Hz, H3), 7.32–7.20 (m, 3H, PPh₃), 7.13 (td, 6H, $J = 7.6$, 1.8 Hz, PPh₃), 6.89–6.74 (m, 6H, PPh₃), 4.95 (s, 5H, $\eta^5\text{-C}_5\text{H}_5$). MS (ESI): m/z [M - PF₆] $^+$ calcd for $\text{C}_{33}\text{H}_{28}\text{N}_2\text{P}_2\text{Ru}$ 609.10, found 609.15. Anal. Calcd for $\text{C}_{33}\text{H}_{28}\text{F}_6\text{N}_2\text{P}_2\text{Ru}$: C, 55.78; H, 3.75; N, 3.72. Found: C, 55.95; H, 3.60; N, 3.38.

Ru4, $[(\eta^5\text{-C}_5\text{H}_5)\text{Ru}(1\text{-}N\text{-}N)(\text{PPh}_3)]_2[\text{PF}_6]_2$. $\eta = 74\%$. Orange. $^1\text{H NMR}$ (300 MHz, DMSO): δ 9.51 (br. s, 1H, H2), 9.30 (d, 1H, $J = 5.6$ Hz, H5), 8.72 (s, 1H, H8), 8.55 (d, 1H, $J = 8.9$ Hz, H6'), 7.86 (t, 1H, $J = 7.7$ Hz, NH), 7.73 (d, 1H, $J = 7.4$ Hz, H4), 7.47–7.15 (m, 10H, PPh₃ + H3), 7.15–6.90 (m, 6H, PPh₃), 6.42 (d, 1H, $J = 8.9$ Hz, H5'), 4.67 (s, 5H, $\eta^5\text{-C}_5\text{H}_5$), 4.58 (t, 2H, $J = 7.0$ Hz, H10), 3.54 (br. s, 2H, H12), 2.31–2.15 (m, 2H, H11). MS (ESI): m/z [M - PF₆] $^+$ calcd for $\text{C}_{39}\text{H}_{36}\text{N}_8\text{O}_3\text{P}_2\text{Ru}$ 795.15, found 795.11. Anal. Calcd for $\text{C}_{39}\text{H}_{36}\text{F}_6\text{N}_8\text{O}_3\text{P}_2\text{Ru}$: C, 49.85; H, 3.65; N, 11.92. Found: C, 49.86; H, 3.88; N, 11.94.

Ru5, $[(\eta^5\text{-C}_5\text{H}_5)\text{Ru}(2,2'\text{-bipyridyl})(2\text{-}P)]_2[\text{PF}_6]_2$. $\eta = 71\%$. Reddish orange. $^1\text{H NMR}$ (300 MHz, DMSO): δ 9.53 (s, 1H, NHCO), 9.37 (d, 2H, $J = 5.5$ Hz, H2 bipy), 8.59 (t, 1H, $J = 5.6$ Hz, NH), 8.51 (d, 1H, $J = 9.0$ Hz, H6'), 8.18 (d, 2H, $J = 8.1$ Hz, H5 bipy), 7.84 (t, 2H, $J = 7.7$ Hz, H4 bipy), 7.71 (d, 2H, $J = 7.1$ Hz, H3), 7.41 (dd, 2H, $J = 7.6$, 6.1 Hz, H3 bipy), 7.36–7.23 (m, 6H, PPh₂ + H2), 7.06 (t, 2H, $J = 9.0$ Hz, PPh₂), 6.98–6.83 (m, 4H, PPh₂), 6.42 (d, 1H, $J = 9.0$ Hz, H5'), 4.89 (s, 5H), 3.55 (s, 2H, H7), 3.43–3.32 (m, 2H, H9), 2.01–1.86 (m, 2H, H8). MS (ESI): m/z [M - PF₆] $^+$ calcd for $\text{C}_{43}\text{H}_{37}\text{N}_7\text{O}_4\text{P}_2\text{Ru}$ 848.17, found 848.20. Anal. Calcd for $\text{C}_{43}\text{H}_{37}\text{F}_6\text{N}_7\text{O}_4\text{P}_2\text{Ru}$: C, 52.02; H, 3.76; N, 9.88. Found: C, 52.23; H, 3.58; N, 9.34.

Synthesis of Ru3. $[(\eta^5\text{-C}_5\text{Me}_5)\text{Ru}(1,10\text{-phenanthroline})(\text{PPh}_3)]_2[\text{PF}_6]_2$. CH_2Cl_2 (15 mL) was added to a Schlenk tube charged with $[(\eta^5\text{-C}_5\text{Me}_5)\text{RuCl}(\text{PPh}_3)_2]_2[\text{PF}_6]_2$ (80 mg, 0.10 mmol) and AgPF₆ (27 mg, 0.11 mmol). After the mixture had been stirred for 30 min, 1,10-phenanthroline (20 mg, 0.11 mmol) was added, and the mixture was stirred overnight at room temperature. The solution was then filtered and pumped to dryness, and the crude was washed with *n*-hexane (10 mL) and ethyl ether (10 mL). The crude product was dissolved in acetone (5 mL), filtered, and pumped to dryness. The product was recrystallized by slow diffusion of ethyl ether in a dichloromethane solution. $\eta = 73\%$. Red. $^1\text{H NMR}$ (300 MHz, DMSO): δ 9.36 (d, 2H, $J = 5.0$ Hz, H2), 8.46 (d, 2H, $J = 8.1$ Hz, H3), 7.94 (s, 2H, H5), 7.90 (dd, 2H, $J = 8.0$, 5.3 Hz, H2), 7.24 (br. m, 3H, PPh₃), 7.12 (br. m, 6H, PPh₃), 6.74 (br. m, 6H, PPh₃), 1.39 (s, 15H). MS (ESI): m/z [M - PF₆] $^+$ calcd for $\text{C}_{40}\text{H}_{38}\text{N}_2\text{P}_2\text{Ru}$ 679.18, found 679.06. Anal. Calcd for $\text{C}_{40}\text{H}_{38}\text{F}_6\text{N}_2\text{P}_2\text{Ru}$: C, 58.32; H, 4.65; N, 3.40. Found: C, 58.08; H, 5.03; N, 3.01.

X-ray Diffraction Studies of Ru3. Single-crystal X-ray diffraction (SCXRD) experiments were performed with a Bruker D8 Quest area detector diffractometer. The crystal was mounted on a Kapton loop. A graphite-monochromated Mo $K\alpha$ ($\lambda = 0.71073$ Å) radiation source running at 50 kV and 30 mA was used. An empirical absorption correction was enforced using Bruker SADABS,⁴⁵ and data were reduced with the Bruker SAINT program.⁴⁶ The structure was determined by direct methods with Bruker SHELXS⁴⁷ and refined by full-matrix least-squares on F^2 using SHELXL⁴⁷ programs within WINGX version 2014.1.⁴⁸ Non-hydrogen atoms were refined with anisotropic thermal parameters. Hydrogen atoms were placed in

calculated positions and allowed to be refined in the parent carbon atoms. Structural representation was made using Mercury 3.8.⁴⁹ A summary of the crystal data, structure solution, and refinement parameters is given in Table S1. Collected data are poor due to weak diffraction of the crystal. CCDC 1996562.

Biology. Blood-Stage Antiplasmodial Activity. Sample Preparation. Each compound was solubilized in 100% DMSO (Sigma-Aldrich) to obtain a final concentration of 5 mM. Intermediate dilutions were then prepared as appropriate in parasite culture media.

***P. falciparum* In Vitro Cultures.** Laboratory-adapted *P. falciparum* lines 3D7 (chloroquine-, mefloquine-, and artemisinin-susceptible; IHMT-NOVA culture collection), 3D7-GFP (chloroquine-, mefloquine-, and artemisinin-susceptible; MRA-1029, MR4, ATCC, Manassas, VA), Dd2 (chloroquine- and mefloquine-resistant and artemisinin-susceptible; IHMT-NOVA culture collection), and IPC5202 (artemisinin-resistant; MRA-1240, MR4, ATCC) were continuously cultivated at 5% hematocrit and 37 °C in a 5% CO₂ atmosphere, and human serum was replaced with 0.5% AlbuMAXII (Invitrogen) in the culture medium (RPMIc) and sorbitol synchronized, as previously described.⁵⁰

Dose–Response Assay for IC₅₀ Estimation. An unsynchronized culture with 1% hematocrit and 1% parasitemia was incubated with the tested compounds in 5-fold serial dilutions ranging from 10000 to 0.64 nM. After 72 h at 37 °C in 5% CO₂, cells were diluted to achieve a 0.25% hematocrit and parasite growth was assessed by flow cytometry (Beckman Coulter, Cytoflex) with a 96-well plate reader for each parasite strain as follows. For 3D7-GFP, read directly (green; excitation wavelength, 488 nm); for Dd2 and IPC5202, parasites were stained with 0.5× SYBR green I (Invitrogen, Thermo Fisher Scientific) in PBS for 30 min in the dark, at 37 °C, washed once with PBS, and then read as for 3D7-GFP.^{51,52} To estimate the IC₅₀ values of fluorescent compounds **Ru4** and **Ru5**, the 3D7 strain (not expressing GFP) was used; after the 72 h incubation, parasites were stained with 0.5 μM SYTO61 (Invitrogen, Thermo Fisher Scientific) for 45 min in the dark, at 37 °C, and washed once with PBS, and parasite growth was assessed by flow cytometry (red; SYTO-61; 633 nm, 660/20 nm bandpass).⁵³ Typically, 20000–40000 red blood cells (RBCs) were counted, and samples were analyzed using FlowJo software (Tree Star Inc.). Half-maximal inhibitory concentrations (IC₅₀) were determined with GraphPad Prism 5 (trial version). Values are the average of at least three experiments, each conducted in duplicate.

In Vitro Stage-Dependent Antimalarial Activity. Stage-specific compound treatment effects were elucidated using synchronized (6 h window) parasites in 96-well plates with a starting parasitemia of 1% and a hematocrit of 2%. Parasites were treated with 10-fold IC₅₀ (80 nM) concentrations of **Ru2** or with RPMIc (with <0.0016% DMSO; no drug control), at 3 or 6 h during the intraerythrocytic life cycle: ring stage (6–10 h post-injection) and trophozoite stage (22–24 h post-injection). After being incubated, washed parasites were also diluted 1:16 and allowed to grow without the drug for two additional cell cycles (96 h). Parasitemia after reinvasion or after growth for 96 h was quantified. Cells were stained with 0.5× SYBR green I (Invitrogen, Thermo Fisher Scientific) and washed with PBS, and parasitemia was assessed by flow cytometry (Cytoflex, Beckman-Coulter; green; 488 nm excitation, emission 530/30 nm bandpass) collecting data from 20000–40000 RBCs. Values are the average of at least three experiments, each conducted in duplicate.

Confocal Microscopy Studies. One milliliter of a *P. falciparum* 3D7 asynchronous cell suspension (2% hematocrit, ≈3% parasitemia) was stained with 0.5 μM **Ru4** or **Ru5** in PBS. After a 5 min incubation (at 37 °C, 5% humidity, and 5% CO₂), ≤1 μg/mL WGA-Alexa 633 (1:2 dilution from the original stock) and 5 μg/mL Hoechst 33342 (Invitrogen, Thermo Fisher Scientific) dye were added and the mixture was incubated for 10 min. Wheat germ agglutinin-Alexa 633 was purchased from Thermo Fisher Scientific.⁵⁴ Hoechst 33342 (Invitrogen, Thermo Fisher Scientific) is a lipophilic DNA-binding fluorescent stain. After WGA-Alexa 633 and Hoechst 33342 destaining protocols, the samples were washed to remove the unbound

dye. Specifically, 1 mL of the incubated solution was centrifuged, the supernatant was discarded, and cells were washed once in 1 mL of PBS. After the last centrifugation, the supernatant was discarded, the cell pellet was resuspended in 1 mL of PBS, and 200 μL of the cell suspension was placed in eight-well chambered coverslips (Ibidi GmbH, Munich, Germany). The cells were then imaged by a CLSM using the 488 nm Ar⁺ laser line (**Ru4** and **Ru5** images) and the 633 nm He–Ne laser line (Alexa 633 images). Hoescht 3342 images were recorded in the multiphoton mode under 780 nm excitation, and hemozoin was visualized using the laser reflection mode. A Leica TCS SPS inverted microscope with a 63× water (1.2 numerical aperture) apochromatic objective was used. Images were collected with 512 × 512 pixels at a scan rate of 100 Hz laser. Images were processed with LAS AF Lite, Fiji, and Wright Cell Imaging Facility (WCIF) ImageJ software.

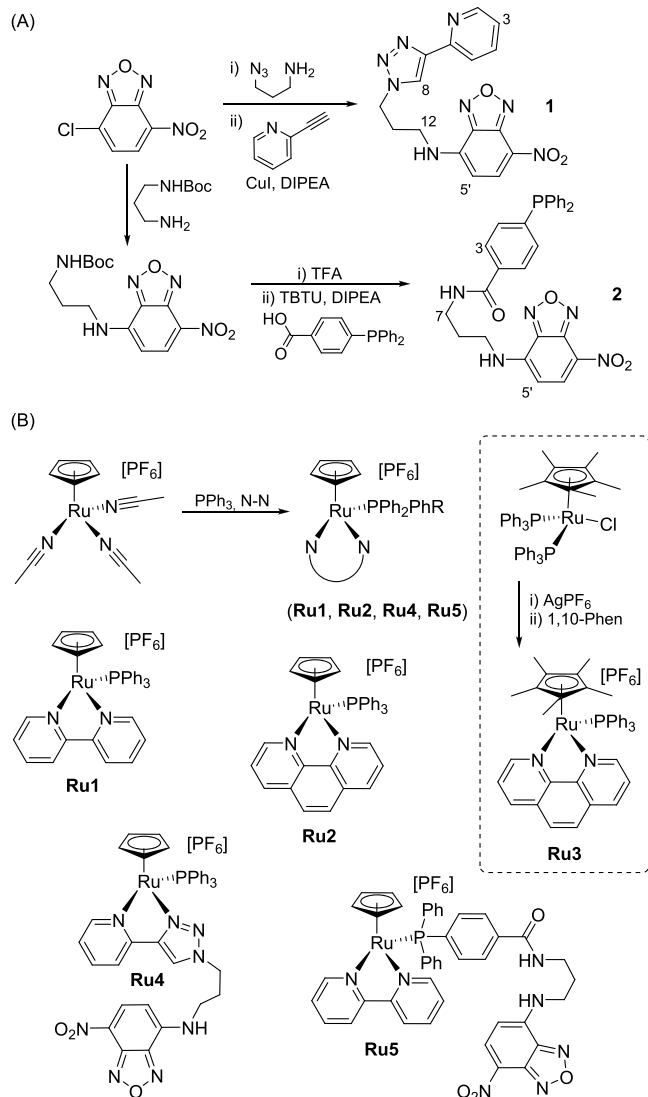
HepG2 Dose–Response Assay. The viability of HepG2 cells was determined after their exposure to compounds for 48 h by the MTT [3-(4,5-dimethylthiazol-2-yl)-2,5-diphenyltetrazolium bromide (Sigma)] assay.⁵⁵ Briefly, 5000 HepG2 cells per well (ATCC HB-8065) were cultured in 96-well plates (Corning Primaria) and allowed to attach for 24 h before the addition of several concentrations of compounds (20 and 50 μM for preliminary screening and 0, 2, 5, 8, 10, 12, 15, 18, and 20 μM for CC₅₀ determination). Compounds were incubated for 48 h at 37 °C. MTT was added to plates at a final concentration of 400 mg/mL per well, followed by incubation at 37 °C for 3 h. After incubation, medium was removed, and formazan crystals were dissolved in a 4:1 dimethyl sulfoxide/glycine buffer (pH 10.5). Plates were shaken for 15 min, and cell viability was then assessed by measuring formazan absorption at 550 nm. Nonlinear regression analysis was employed to fit the normalized results of the dose–response curves, and CC₅₀ values were determined using GraphPad Prism 5 (trial version).

Compound Activity against the Hepatic Stage of Plasmodium Infection In Vitro. Huh-7 cells, a human hepatoma cell line, were cultured in 1640 rpmI medium supplemented with 10% (v/v) fetal calf serum (FCS), 1% (v/v) non-essential amino acids, 1% (v/v) penicillin/streptomycin, 1% (v/v) glutamine, and 10 mM HEPES (pH 7) and maintained at 37 °C with 5% CO₂. Inhibition of *Plasmodium berghei* hepatic infection was determined by measuring the luminescence of Huh-7 cell lysates 48 h after infection with a firefly luciferase-expressing *P. berghei* line, PbGFP-Luccon, as previously described.^{56,57} Briefly, Huh-7 cells (1 × 10⁴ cells per well) were seeded in 96-well plates the day before drug treatment and infection. Stock solutions (10 mM) of the compounds were obtained by dissolving in DMSO, and dilutions were subsequently performed employing infection medium (culture medium supplemented with 50 μg/mL gentamicin and 0.8 μg/mL amphotericin B) to the desired concentration. One hour prior to infection, the culture medium was replaced with fresh infection medium containing the appropriate concentration of each compound. Sporozoites (1 × 10⁴ per well), freshly obtained through disruption of salivary glands of infected female *Anopheles stephensi* mosquitoes, were added to the wells 1 h after compound addition. Sporozoite addition was followed by centrifugation at 1800g for 5 min. The effect of the compounds on the viability of Huh-7 cells was assessed 46 h post-infection by the AlamarBlue assay (Invitrogen), according to the manufacturer's protocol. The parasite load was determined 48 h after infection by a bioluminescence assay (Biotium), according to the manufacturer's recommendations. Nonlinear regression analysis was employed to fit the normalized results of the dose–response curves, and IC₅₀ values were determined using GraphPad Prism 8.0 (GraphPad Software, La Jolla, CA).

RESULTS AND DISCUSSION

Synthesis and Characterization. 7-Nitrobenzoxadiazole (NBD)-appended fluorescent ligands [**1** and **2** (Scheme 1A)] were obtained via 4-propylamine-NBD derivatives functionalized with either azide for (3+2) Cu(I)-catalyzed cycloaddition with 2-ethynylpyridine (**1**) or amine for condensation

Scheme 1. Synthesis of NBD-Labeled Ligands 1 and 2, with (A) the Numbering Scheme and (B) Organometallic Compounds Ru1–Ru5



with 4-diphenylphosphine benzoic acid (2). Organoruthenium(II) compounds of the general formula $[(\eta^5\text{-C}_5\text{R}_5)\text{Ru}(\text{PPh}_3)(\text{N-N})][\text{PF}_6]$ were obtained in one step from commercially available ruthenium parent compounds

$[(\eta^5\text{-C}_5\text{H}_5)\text{Ru}(\text{NCCH}_3)_3][\text{PF}_6]$ (**Ru1**, **Ru2**, **Ru4**, and **Ru5**) and $[(\eta^5\text{-C}_5\text{Me}_5)\text{Ru}(\text{PPh}_3)_2\text{Cl}][\text{PF}_6]$ (**Ru3**) (Scheme 1B).

Compounds **1**, **2**, and **Ru1–Ru5** were characterized by ^1H NMR, LC-MS, and elemental analysis. ^1H NMR spectra of the organometallic complexes display a sharp singlet attributed to the cyclopentadienyl ring, between 4.67 and 4.95 ppm for $\eta\text{-C}_5\text{H}_5$ (Cp) derivatives **Ru1**, **Ru2**, **Ru4**, and **Ru5** and at 1.39 ppm for $\eta\text{-C}_5\text{Me}_5$ (Cp*) compound **Ru3**, multiplets in the aromatic region attributed to the triphenylphosphine ligands (6.70–7.30 ppm), and the signals corresponding to the nitrogen quelaate ligands, in agreement with proposed structures of the complexes. Mass spectra of the compounds confirmed the complex formulations, with complex spectra displaying the distinctive isotopic pattern of ruthenium. Elemental analyses of compounds are also in agreement with the proposed formulations, except for compounds **1** and **Ru5**, for which the nitrogen values differ by 1.76% and 0.54%, respectively. Nonetheless, LC-MS analysis supports the purity of both compounds (Figures S8 and S9). Fluorescent complexes **Ru4** and **Ru5**, developed to visually probe parasitic absorption/distribution (*vide infra*), were further studied by fluorescence spectroscopy, revealing λ_{em} values of 553 nm ($\lambda_{\text{ex}} = 462$ nm) and 555 nm ($\lambda_{\text{ex}} = 474$ nm), respectively.

Compound **Ru3** was further characterized by X-ray diffraction. The asymmetric unit includes a cationic complex and a PF_6^- anion that is severely disordered. The cation of **Ru3** (Figure S10) adopts a “three-legged piano stool” geometry, with the ruthenium atom bonded to the phenanthroline nitrogen and the PPh_3 phosphorus atom (piano stool legs), and the η -coordinated pentamethylcyclopentadienyl (piano stool seat). The Ru–N bond lengths for **Ru3** [2.115(4) and 2.124(4) Å (Table S2)] are in the upper range of Ru–N bond lengths found for similar ruthenium complexes (1.992–2.176 Å).⁵⁸ The Ru–P and Ru–Cp^c (superscript c = centroid) bond lengths [2.3484(13) and 1.8420(5) Å, respectively] are also within the ranges of similar compounds of this type (2.277–2.359 Å for Ru–P bond lengths and 1.854–1.84 Å for Ru–Cp^c bond lengths). The N–Ru–N angle (Table S2), dependent on phenanthroline bite, is 77.24(18)° for the **Ru3** cation, similar to those of other ruthenium phenanthroline complexes (77.137–77.787°), whereas the P–Ru–N angles are 88.08(11)° and 90.54(12)°, which lie at the bottom of the array found for other complexes found in the CCSD (87.669–97.297°).⁵⁸ Structural inspection of **Ru3** revealed steric hindrance between Cp* methyl groups and PPh_3 phenyl rings, with H–H interligand contacts as short as 2.007 Å,

Table 1. *In Vitro* Antiplasmodial Activity (blood stage) and Cytotoxicity (HepG2) of Ruthenium Compounds^a

	<i>P. falciparum</i> (blood stage) IC ₅₀ (nM)				HepG2 CC ₅₀ (μM)	RI	SI
	3D7-GFP	3D7 ^b	Dd2	IPC5202			
Ru1	9.6 ± 3.0	nd	53 ± 25	83 ± 9	10.8 ± 0.6	6, 9	1125, 204, 130
Ru2	7.69 ± 0.22	nd	60 ± 30	68 ± 14	6.1 ± 0.7	8, 9	793, 101, 89
Ru3	12 ± 6	nd	71 ± 16	78 ± 4	7 ± 1	6, 6	583, 99, 90
Ru4	219 ± 62	464 ± 35	325 ± 116	939 ± 299	>50	1.5, 4.2	>228, >154, >53
Ru5	139 ± 54	167 ± 14	174 ± 34	209 ± 64	>50	1.2, 1.5	>360, >299, >239
DHA	14.40 ± 0.01	nd	29 ± 9	46 ± 12	>1000	2.0, 3.2	>71 × 10 ³ , >34 × 10 ³ , >21 × 10 ³
CQ	15.8 ± 0.8	nd	340 ± 21	54 ± 3	>200	22, 3.4	>14 × 10 ³ , >7 × 10 ³ , >4 × 10 ³
PQ	244 ± 15	nd	585 ± 42	880 ± 116	nd	2.4, 3.6	nd

^aLigands **1**, **2**, and PPh_3 were evaluated against the 3D7-GFP *Pf* strain at 1 μM, revealing inhibitions of 0%, 49.9%, and 2.7%, respectively. RI (resistance index) = $\text{IC}_{50}(\text{Dd2}, \text{IPC5202})/\text{IC}_{50}(\text{3D7-GFP})$. SI (selectivity index) = $\text{IC}_{50}(\text{HepG2})/\text{IC}_{50}(\text{3D7-GFP}, \text{Dd2}, \text{IPC5202})$. ^bFluorescent compounds **Ru4** and **Ru5** were also studied in the nonfluorescent 3D7 strain. nd = not determined.

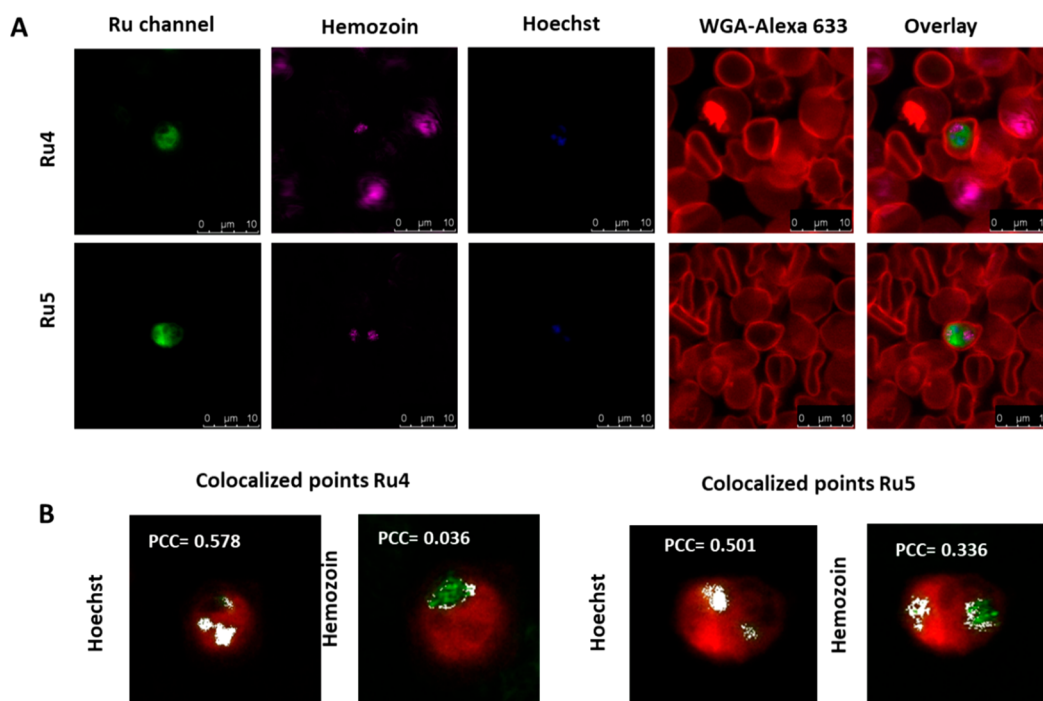


Figure 4. CLSM-based distribution analysis of **Ru4** and **Ru5** (green channel). (A) Representative CLSM images of RBCs and iRBCs stained with **Ru4** or **Ru5**, Hoescht (blue channel), and WGA-Alexa 633 dyes (red channel). The parasite's hemozoin (purple channel) was visualized using laser reflection. Overlay images are presented in the right panels. (B) Co-localization images, highlighting the positive signals for both channels (white), and PCC values.

despite the staggered conformation adopted by PPh_3 , explaining the broad shape of PPh_3 ^1H NMR signals (Figure S5). A comparison of the crystal structures of **Ru3** and **Ru2**⁴¹ (see Table S2), which differ only in the cyclopentadienyl ligand (C_5Me_5 and C_5H_5 , respectively), shows longer ruthenium–ligand bond distances for **Ru3**. The larger $\text{Cp}^c\text{–Ru–P}$ angle of **Ru3** [$129.85(4)^\circ$] relative to that of **Ru2** [$125.48(3)^\circ$] evidences the steric hindrance between the bulky Cp^* and PPh_3 ligands, and concomitantly, the quasi-planar phenanthroline ligand is “pushed” toward the Cp^* , as indicated by the smaller $\text{Cp}^{*c}\text{–Ru–N}(1)$ angle [$127.89(11)^\circ$ in **Ru3** vs $131.34(9)^\circ$ in **Ru2**], thus minimizing steric clashes within the **Ru3** coordination sphere.

Blood-Stage Antiplasmodial Activity. Dose–Response Studies. We determined dose–response profiles of compounds **Ru1–Ru5** against the blood stage of CQ-sensitive 3D7-GFP, CQ-resistant Dd2, and artemisinin-resistant IPC5202 *Pf* strains. The antiplasmodial activity (IC_{50}) and cytotoxicity (CC_{50}) of compounds in human hepatic cells (HepG2) as well as their selectivity indices were determined (Table 1). Reference antiplasmodial compounds dihydroartemisinin (DHA), CQ, and primaquine (PQ) were included as controls in these experiments.

Inspection of Table 1 reveals that compounds **Ru1–Ru3** were highly potent against the 3D7-GFP *Pf* strain, with IC_{50} values ranging from 7.69 to 12 nM. To the best of our knowledge, **Ru1** and **Ru2** are the first ruthenium-arene compounds displaying single-digit nanomolar IC_{50} values against this strain. This result contrasts with those reported for hybrid ruthenium(II) complexes of chloroquine, which were shown to be significantly less active against the 3D7-GFP *Pf* strain (IC_{50} values ranging from 0.02 to $0.34\ \mu\text{M}$).^{32,39} NBD-appended complexes **Ru4** and **Ru5** were less active, with IC_{50} values of 219 and 139 nM, respectively. The IC_{50} values of

Ru4 and **Ru5** against a nonfluorescent 3D7 *Pf* strain confirmed that NBD fluorescence does not markedly influence *Pf* 3D7 fluorescence-based analysis of compound activity and, consequently, the results observed with the GFP-expressing 3D7 *Pf* strain. All compounds revealed lower activity against the CQ-resistant Dd2 *Pf* strain than against the nonresistant 3D7-GFP *Pf* strain, but with IC_{50} values and resistance indices lower than those of CQ. Compounds **Ru1–Ru3** display the first two-digit nanomolar IC_{50} values against the Dd2 *Pf* strain reported so far within the ruthenium-arene chemotype (IC_{50} values ranging from 234 nM to $14.1\ \mu\text{M}$)^{31,33–35,37,38} that are similar to those found for a CQ-ruthenocene-trioxane hybrid (62.00 and $51.16\ \mu\text{M}$ with 10% and 17% O_2 atmospheres, respectively).⁵⁹ Despite being less active than compounds **Ru1–Ru3**, compounds **Ru4** and **Ru5** exhibited lower RIs in the Dd2 *Pf* strain. In the artemisinin-resistant *Pf* strain IPC5202, compounds **Ru1–Ru3** showed nonsignificant differences in IC_{50} , presenting high potency but being slightly less active and exhibiting higher RIs than DHA. As observed for the Dd2 strain, **Ru4** and **Ru5** exhibit higher IC_{50} values but lower RIs compared to those of **Ru1–Ru3**. In fact, compound **Ru5** exhibits similar potency against all *Pf* strains tested, with RIs of 1.2 and 1.5 for the Dd2 and IPC5202 *Pf* strains, respectively.

Structurally, these compounds differ from previously reported ruthenium-arene antimalarials in the arene (cyclopentadienyl vs benzene derivatives), the referenced non-hybridization with organic antimalarial motifs, and the coordinated PPh_3 , a ligand known to play a key role in the anticancer activity of cyclopentadienylruthenium(II) compounds.⁴⁰ The lipophilicity induced by the triphenylphosphine in the complex's coordination sphere may have an important role in their high antiplasmodial activities.³³ Nonetheless, it is worth noticing that the higher lipophilicity of **Ru3**, when compared to that of **Ru2**, induced by the bulkier Cp^* ligand,

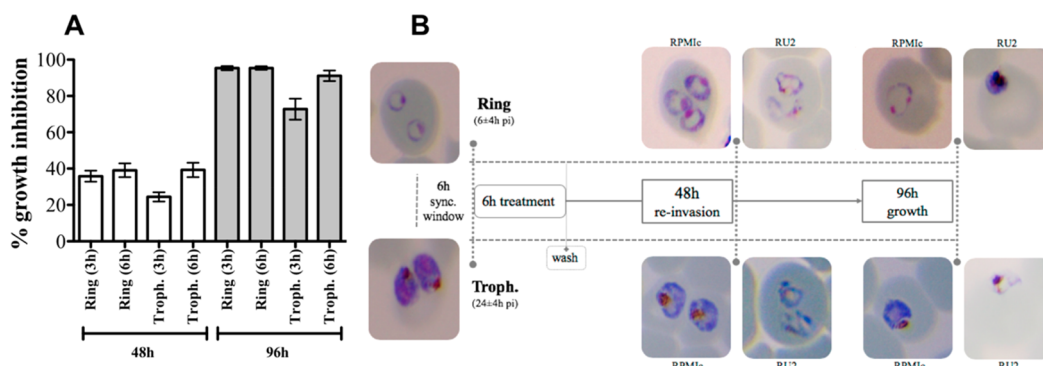


Figure 5. Effect of **Ru2** on the intraerythrocytic cycle of *P. falciparum*. (A) Synchronized 3D7 cultures, with a 6 h window, in ring and trophozoite (Troph.) stages were exposed to drug pulses of 10-fold IC_{50} **Ru2** (80 nM) for 3 and 6 h. The bars represent means and standard errors of the mean of parasite growth under each condition, relative to no drug control, quantified after one cycle (48 h, white bars) and three cycles (96 h, gray bars). (B) Photomicrographs of Giemsa-stained blood smears illustrating parasite morphology before a 6 h pulse of **Ru2** and after 48 and 96 h, in both ring- and trophozoite-stage parasites. RPMic culture medium.

led to neither higher antiplasmodial activity nor higher cytotoxicity.

Compounds **Ru1**–**Ru3** revealed low cytotoxicity against HepG2 cells, as indicated by their CC_{50} values in the low micromolar range (6.1–10.8 μM), with **Ru1** showing an improved cytotoxicity profile when compared to those of **Ru2** and **Ru3**. This was expected, given the previous results of anticancer activity of compounds **Ru1** and **Ru2**,^{40,41} and other compounds within the same scaffold.⁴³ Selectivity indices (SIs) show nonetheless large therapeutic windows for these compounds, even against the least sensitive strain (IPC5202), for which SIs ranged between 89 and 130. Compounds **Ru4** and **Ru5** exhibited less cytotoxicity in HepG2 cells than their **Ru1**–**Ru3** counterparts did, with CC_{50} values of >50 μM , indicating good SI values also for these compounds.

Cellular Localization Studies. Exploiting the intrinsic fluorescence of NBD-appended compounds, we next evaluated cellular localization of **Ru4** and **Ru5** in *P. falciparum* using a co-staining protocol together with confocal microscopy images. Images from confocal laser scanning microscopy (CLSM) reveal that **Ru4** and **Ru5** accumulate only inside infected red blood cells (iRBCs) and are largely dispersed throughout the parasite's cytoplasm after incubation for 15 min (Figure 4A). The degree of co-localization of **Ru4** and **Ru5** in the nucleus and hemozoin-containing digestive vacuole, determined by calculation of Pearson's correlation coefficients (PCCs) (Figure 4B),⁶⁰ shows that both compounds accumulate mainly inside the parasite's nucleus (Figure 4B, Hoescht), with high PCCs obtained in both cases (0.578 and 0.501 for **Ru4** and **Ru5**, respectively). Nuclear accumulation is further supported by intensity profile analysis (Figure S11), which showed a similar spatial distribution of **Ru4** and **Ru5** with the nucleus. Importantly, in addition to the nucleus, **Ru5** significantly accumulates inside the hemozoin-containing digestive vacuole [PCC = 0.336 (Figure 4B)]. The fact that the NBD derivative ligand **2**, but not ligand **1** or PPh_3 (Table 1), showed significant blood-stage antiplasmodial activity (49.9% inhibition at 1 μM) suggests ligand **2**-induced digestive vacuole accumulation and indicates tunability within the cyclopentadienylruthenium(II) scaffold by complex ligand-sphere variation. Interestingly, compounds within the $[(\eta^5-C_5H_5)Ru(PPh_3)(N-N)]^+$ scaffold are known to accumulate mostly in mammalian cancer cell membranes,⁴³ indicating that

compounds must be selectively absorbed via a *Plasmodium*-specific uptake mechanism, without affecting erythrocytes at the tested concentration.

Antiplasmodial Activity in a Synchronized *P. falciparum* Culture. Following the establishment of the compound's activity against *Pf* blood stages (Table 1), the activity of compound **Ru2** against the erythrocytic stage of the parasite's life cycle was investigated in a tightly synchronized *Pf* culture (3D7). Parasitemia and parasite development were analyzed by flow cytometry and by Giemsa-stained thin blood smears (Figure 5). The *in vitro* speed of action of **Ru2** was assessed by incubation of synchronized parasites at the ring and trophozoite stages in the presence of a 10-fold IC_{50} concentration of the compound. Parasites were challenged for 3 and 6 h periods and, following drug removal, were allowed to resume growth in drug-free culture medium. After completion of one maturation cycle (48 h), **Ru2** induced a modest decrease in total parasitemia of <50%, indicating only a moderate impairment of reinvasion against both ring and trophozoite stages (Figure 5A). In contrast, after growing for 96 h in the absence of the drug, the parasites were still unable to resume growth, with an inhibition effect of almost 100% under all conditions (Figure 5A). This indicates that, regardless of the stage of development, **Ru2** can induce irreversible damage to the parasite cell after contact with the parasite for only 3 or 6 h, strongly suggesting a cytotoxic mode of action. A considerable fraction of parasites, both during the initial 48 and 96 h of recovery, lacked the characteristic morphology of rings or trophozoites and were instead severely perturbed, with a vast majority showing a lack of DNA and/or organized nucleus, and hyaline, vacuolated and dispersed cytoplasm (Figure 5B).⁶¹ Particularly at 96 h, the very few parasites observed were debris-like forms or very condensed crisis forms (Figure 5B). These results indicate that **Ru2** impairs asexual parasite differentiation, exhibiting fast parasitocidal activity against both the ring and trophozoite stages of *Pf*.

Liver-Stage Antiplasmodial Activity. Compounds were further evaluated for their ability to inhibit the invasion and development of *Plasmodium* parasites in liver cells, using an *in vitro* infection model that employs a human hepatoma cell line (Huh7) infected with firefly luciferase-expressing *P. berghei* rodent malaria parasites.^{56,57} IC_{50} values are listed in Table 2,

and representative dose–response curves are shown in Figure S12.

Table 2. *In Vitro* Antiplasmodial Activity (liver stage) of Ruthenium Compounds

	<i>P. berghei</i> IC ₅₀ (μM)
Ru1	0.33 ± 0.14
Ru2	0.451 ± 0.010
Ru3	1.33 ± 0.25
Ru4	2.68 ± 0.69
Ru5	4.20 ± 1.47
ATV ⁶²	0.0011
PQ ⁶²	9.5

Notably, ruthenium compounds were able to significantly affect hepatic infection, with IC₅₀ values within the range of 0.33–4.20 μM. **Ru1** and **Ru2** presented the best activities, displaying IC₅₀ values of 0.33 and 0.451 μM, respectively (nonsignificant difference). In contrast to what was observed against the blood-stage infection of *Pf* strains, **Ru3** was found to be less active against the liver stage of infection than its **Ru1** and **Ru2** counterparts, with **Ru4** and **Ru5** again displaying the lowest activity. While all compounds are thus much less active than atovaquone (ATV), an inhibitor of the parasite's cytochrome *bc*₁ with potent liver-stage activity,⁶³ they were shown to be significantly more effective than primaquine, the gold standard for targeting liver-stage parasites, which requires metabolic activation to exert its effect.⁶⁴ Compounds are thus more active than other ruthenium-arene compounds against the liver stage of *P. berghei* (50% inhibition at 10 μM).³⁹ The confluency of Huh7 hepatoma cells was not affected within the compound concentration ranges used for IC₅₀ determinations, demonstrating the absence of cytotoxicity under the experimental conditions employed (Figure S12).

CONCLUSIONS

Herein, we report “half-sandwich” cyclopentadienylruthenium(II) compounds of the general formula [(η⁵-C₅R₅)Ru(PPh₃)-(N-N)][PF₆], a scaffold tested for the first time as an antiplasmodial agent. Compounds displayed very high potency against the blood stage of *P. falciparum*, with the most potent compounds revealing single-digit nanomolar activity (IC₅₀) in 3D7-GFP and low nanomolar activity in CQ-resistant Dd2 and artemisinin-resistant IPC5202 strains, while showing residual cytotoxicity in hepatic cells (HepG2). In the liver stage of *P. berghei*, the best compounds (**Ru1** and **Ru2**) exhibited submicromolar antiplasmodial activity with no toxicity to hepatic host cells (Huh7). Confocal microscopy studies uncovered parasite-selective absorption of NBD-labeled compounds **Ru4** and **Ru5** in 3D7-infected erythrocytes, and parasite nuclear accumulation of both compounds, with accumulation of **Ru5** also in the hemozoin-containing digestive vacuole. Lead compound **Ru2** revealed impairment of asexual differentiation in a blood-stage 3D7 *P. falciparum*-synchronized strain, and fast parasitocidal activity against both ring- and trophozoite-stage parasites. These compounds rank among the best metalloantimalarials¹⁸ reported so far^{16–18,29–39} and are especially relevant considering the nonhybridization with organic antimalarial drugs. Overall, these results highlight the cyclopentadienylruthenium(II) scaffold as a promising antiplasmodial chemotype and are expected to inspire others in the discovery of new, “out-of-the-box” metallo-antiplasmodials.

ASSOCIATED CONTENT

Supporting Information

The Supporting Information is available free of charge at <https://pubs.acs.org/doi/10.1021/acs.inorgchem.0c01795>.

¹H NMR spectra of compounds **1**, **2**, and **Ru1–Ru5**; X-ray crystal data, structural refinement parameters, and molecular diagram for **Ru3**; and confocal microscopy intensity profile analysis of **Ru4** and **Ru5** (PDF)

Accession Codes

CCDC 1996562 contains the supplementary crystallographic data for this paper. These data can be obtained free of charge via www.ccdc.cam.ac.uk/data_request/cif, or by emailing data_request@ccdc.cam.ac.uk, or by contacting The Cambridge Crystallographic Data Centre, 12 Union Road, Cambridge CB2 1EZ, UK; fax: +44 1223 336033.

AUTHOR INFORMATION

Corresponding Author

Pedro R. Florindo – Instituto de Investigação do Medicamento (iMed.U LISBOA), Faculdade de Farmácia, Universidade de Lisboa, 1649-003 Lisboa, Portugal; orcid.org/0000-0002-8582-7036; Email: pedrorflorindo@ff.ulisboa.pt

Authors

Sofia A. Milheiro – Instituto de Investigação do Medicamento (iMed.U LISBOA), Faculdade de Farmácia, Universidade de Lisboa, 1649-003 Lisboa, Portugal

Joana Gonçalves – Instituto de Investigação do Medicamento (iMed.U LISBOA), Faculdade de Farmácia, Universidade de Lisboa, 1649-003 Lisboa, Portugal

Ricardo M. R. M. Lopes – Instituto de Investigação do Medicamento (iMed.U LISBOA), Faculdade de Farmácia, Universidade de Lisboa, 1649-003 Lisboa, Portugal

Margarida Madureira – Instituto de Investigação do Medicamento (iMed.U LISBOA), Faculdade de Farmácia, Universidade de Lisboa, 1649-003 Lisboa, Portugal

Lis Lobo – Department of Medical Parasitology, Global Health and Tropical Medicine, GHTM, Instituto de Higiene e Medicina Tropical, IHMT, Universidade Nova de Lisboa, 1349-008 Lisboa, Portugal

Andreia Lopes – Department of Medical Parasitology, Global Health and Tropical Medicine, GHTM, Instituto de Higiene e Medicina Tropical, IHMT, Universidade Nova de Lisboa, 1349-008 Lisboa, Portugal

Fátima Nogueira – Department of Medical Parasitology, Global Health and Tropical Medicine, GHTM, Instituto de Higiene e Medicina Tropical, IHMT, Universidade Nova de Lisboa, 1349-008 Lisboa, Portugal; orcid.org/0000-0003-0313-0778

Diana Fontinha – Instituto de Medicina Molecular João Lobo Antunes, Faculdade de Medicina, Universidade de Lisboa, 1649-028 Lisboa, Portugal

Miguel Prudêncio – Instituto de Medicina Molecular João Lobo Antunes, Faculdade de Medicina, Universidade de Lisboa, 1649-028 Lisboa, Portugal

M. Fátima M. Piedade – Centro de Química Estrutural, Instituto Superior Técnico, Universidade de Lisboa, 1049-001 Lisboa, Portugal; Departamento de Química e Bioquímica, Faculdade de Ciências da Universidade de Lisboa, 1749-016 Lisboa, Portugal

Sandra N. Pinto – *iBB-Institute for Bioengineering and Biosciences, Department of Bioengineering, Instituto Superior Técnico, Universidade de Lisboa, 1049-001 Lisboa, Portugal*
Rui Moreira – *Instituto de Investigação do Medicamento (iMed.Ulisboa), Faculdade de Farmácia, Universidade de Lisboa, 1649-003 Lisboa, Portugal; orcid.org/0000-0003-0727-9852*

Complete contact information is available at:
<https://pubs.acs.org/10.1021/acs.inorgchem.0c01795>

Notes

The authors declare no competing financial interest.

ACKNOWLEDGMENTS

The authors thank Fundação para a Ciência e Tecnologia (FCT) for financial support, through Projects PTDC/MED-QUI/31468/2017 (P.R.F., S.A.M., J.G., M.F.M.P., and R.M.), PTDC/MED-QUI/30021/2017 (R.M., F.N., L.L., and A.L.), UIDB/04565/2020, SAICTPAC/0019/2015, PPBI-POCI-01-0145-FEDER-022122 (S.N.P.), UID/Multi/04413/2013 (F.N., L.L., and A.L.), and PTDC/SAU-INF/29550/2017 (M.P.) and Grant SFRH/BD/121664/2016 (R.M.R.M.L.). The authors thank MR4 for providing malaria parasites contributed by Didier Menard, Institut Pasteur du Cambodge.

REFERENCES

- (1) World Health Organization. World Malaria Report 2019.
- (2) Rodrigues, T.; Prudêncio, M.; Moreira, R.; Mota, M. M.; Lopes, F. Targeting the Liver Stage of Malaria Parasites: A Yet Unmet Goal. *J. Med. Chem.* **2012**, *55*, 995–1012.
- (3) Capela, R.; Moreira, R.; Lopes, F. An Overview of Drug Resistance in Protozoal Diseases. *Int. J. Mol. Sci.* **2019**, *20*, 5748.
- (4) Mathenge, P. G.; Low, S. K.; Vuong, N. L.; Mohamed, M. Y. F.; Faraj, H. A.; Alieldin, G. I.; Al Khudari, R.; Yahia, N. A.; Khan, A.; Diab, O. M.; Mohamed, Y. M.; Zayan, A. H.; Tawfik, G. M.; Huy, N. T.; Hirayama, K. Efficacy and resistance of different artemisinin-based combination therapies: a systematic review and network meta-analysis. *Parasitol. Int.* **2020**, *74*, 101919.
- (5) Gambino, D.; Otero, L. Perspectives on what ruthenium-based compounds could offer in the development of potential antiparasitic drugs. *Inorg. Chim. Acta* **2012**, *393*, 103–114.
- (6) Dilruba, S.; Kalayda, G. V. Platinum-based drugs: past, present and future. *Cancer Chemother. Pharmacol.* **2016**, *77*, 1103–1124.
- (7) Mirzadeh, N.; Reddy, T.; Bhargava, S. Advances in diphosphine ligand-containing gold complexes as anticancer agents. *Coord. Chem. Rev.* **2019**, *388*, 343–359.
- (8) For recent advances in metal drug discovery, see: Franz, K.; Metzler-Nolte, N. Introduction: Metals in Medicine. *Chem. Rev.* **2019**, *119*, 727–729.
- (9) Yufanyi, D. M.; Abbo, H. S.; Titinchi, S. J. J.; Neville, T. Platinum(II) and Ruthenium(II) complexes in medicine: Antimycobacterial and Anti-HIV activities. *Coord. Chem. Rev.* **2020**, *414*, 213285.
- (10) Zeng, L.; Gupta, P.; Chen, Y.; Wang, E.; Ji, L.; Chao, H.; Chen, Z.-S. The development of anticancer ruthenium(II) complexes: from single molecule compounds to nanomaterials. *Chem. Soc. Rev.* **2017**, *46*, 5771–5804.
- (11) Brabec, V.; Kasparkova, J. Ruthenium coordination compounds of biological and biomedical significance. DNA binding agents. *Coord. Chem. Rev.* **2018**, *376*, 75–94.
- (12) Ko, C.-N.; Li, G.; Leung, C.-H.; Ma, D.-L. Dual function luminescent transition metal complexes for cancer theranostics: The combination of diagnosis and therapy. *Coord. Chem. Rev.* **2019**, *381*, 79–103.
- (13) Yu, Y.; Xu, Q.; He, S.; Xiong, H.; Zhang, Q.; Xu, W.; Ricotta, V.; Bai, L.; Zhang, Q.; Yu, Z.; Ding, J.; Xiao, H.; Zhou, D. Recent advances in delivery of photosensitive metal-based drugs. *Coord. Chem. Rev.* **2019**, *387*, 154–179.
- (14) Imberti, C.; Sadler, P. J. 150 years of the periodic table: New medicines and diagnostic agents. In *Medicinal Chemistry*; Sadler, P. J., van Eldik, R., Eds.; Academic Press (Elsevier): Cambridge, U.K., 2020; pp 3–56.
- (15) Patra, M.; Gasser, G. The medicinal chemistry of ferrocene and its derivatives. *Nat. Rev. Chem.* **2017**, *1*, 0066.
- (16) Xiao, J.; Sun, Z.; Kong, F.; Gao, F. Current scenario of ferrocene-containing hybrids for antimalarial activity. *Eur. J. Med. Chem.* **2020**, *185*, 111791.
- (17) Biot, C.; Castro, W.; Botté, C. Y.; Navarro, M. The therapeutic potential of metal-based antimalarial agents: implications for the mechanism of action. *Dalton Trans.* **2012**, *41*, 6335.
- (18) Salas, P. F.; Herrmann, C.; Orvig, C. Metalloantimalarials. *Chem. Rev.* **2013**, *113*, 3450–3492.
- (19) Bergamo, A.; Gaidon, C.; Schellens, J.; Beijnen, J. H.; Sava, G. Approaching tumour therapy beyond platinum drugs: status of the art and perspectives of ruthenium drug candidates. *J. Inorg. Biochem.* **2012**, *106*, 90–99.
- (20) Li, X.; Gorle, A. K.; Sundaraneedi, M. K.; Keene, F. R.; Collins, J. G. Kinetically-inert polypyridylruthenium(II) complexes as therapeutic agents. *Coord. Chem. Rev.* **2018**, *375*, 134–147.
- (21) Meier-Menches, S. M.; Gerner, C.; Berger, W.; Hartinger, C. G.; Keppler, B. K. Structure-activity relationships for ruthenium and osmium anticancer agents - towards clinical development. *Chem. Soc. Rev.* **2018**, *47*, 909–928.
- (22) Aird, R. E.; Cummings, J.; Ritchie, A. A.; Muir, M.; Jodrell, D. I.; Morris, R. E.; Chen, H.; Sadler, P. J. In vitro and in vivo activity and cross resistance profiles of novel ruthenium (II) organometallic arene complexes in human ovarian cancer. *Br. J. Cancer* **2002**, *86*, 1652–1657.
- (23) Hayward, R. L.; Schornagel, Q. C.; Tente, R.; Macpherson, J. S.; Aird, R. E.; Guichard, S.; Habtemariam, A.; Sadler, P.; Jodrell, D. I. Investigation of the role of Bax, p21/Waf1 and p53 as determinants of cellular responses in HCT116 colorectal cancer cells exposed to the novel cytotoxic ruthenium(II) organometallic agent, RM175. *Cancer Chemother. Pharmacol.* **2005**, *55*, 577–583.
- (24) Scolaro, C.; Bergamo, A.; Brescacin, L.; Delfino, R.; Cocchietto, M.; Laurenczy, G.; Geldbach, T. J.; Sava, G.; Dyson, P. J. In Vitro and in Vivo Evaluation of Ruthenium(II)–Arene PTA Complexes. *J. Med. Chem.* **2005**, *48*, 4161–4171.
- (25) Bergamo, A.; Masi, A.; Dyson, P. J.; Sava, G. Modulation of the metastatic progression of breast cancer with an organometallic ruthenium compound. *Int. J. Oncol.* **2008**, *33*, 1281–1289.
- (26) Meng, X.; Leyva, M. L.; Jenny, M.; Gross, I.; Benosman, S.; Fricker, B.; Harlepp, S.; Hébraud, P.; Boos, A.; Wlosik, P.; Bischoff, P.; Sirlin, C.; Pfeffer, M.; Loeffler, J.-P.; Gaidon, C. A ruthenium-containing organometallic compound reduces tumor growth through induction of the endoplasmic reticulum stress gene CHOP. *Cancer Res.* **2009**, *69*, 5458–5466.
- (27) Klajner, M.; Hébraud, P.; Sirlin, C.; Gaidon, C.; Harlepp, S. DNA Binding to an Anticancer Organo-Ruthenium Complex. *J. Phys. Chem. B* **2010**, *114*, 14041–14047.
- (28) Monro, S.; Colón, K. L.; Yin, H.; Roque, J.; Konda, P.; Gujar, S.; Thummel, R. P.; Lilge, L.; Cameron, C. G.; McFarland, S. A. Transition Metal Complexes and Photodynamic Therapy from a Tumor-Centered Approach: Challenges, Opportunities, and Highlights from the Development of TLD1433. *Chem. Rev.* **2019**, *119*, 797–828.
- (29) Dubar, F.; Egan, T. J.; Pradines, B.; Kuter, D.; Ncokazi, K. K.; Forge, D.; Paul, J.-F.; Pierrot, C.; Kalamou, H.; Khalife, J.; Buisine, E.; Rogier, C.; Vezin, H.; Forfar, I.; Slomianny, C.; Trivelli, X.; Kapishnikov, S.; Leiserowitz, L.; Dive, D.; Biot, C. The antimalarial ferroquine: role of the metal and intramolecular hydrogen bond in activity and resistance. *ACS Chem. Biol.* **2011**, *6*, 275–287.
- (30) Glans, L.; Ehnbo, A.; de Kock, C.; Martínez, A.; Estrada, J.; Smith, P. J.; Haukka, M.; Sánchez-Delgado, R. A.; Nordlander, E. Ruthenium(II) arene complexes with chelating chloroquine analogue

ligands: Synthesis, characterization and in vitro antimalarial activity. *Dalton Trans.* **2012**, *41*, 2764–2773.

(31) Stringer, T.; Quintero, M. A. S.; Wiesner, L.; Smith, G. S.; Nordlander, E. Evaluation of PTA-derived ruthenium(II) and iridium(III) quinoline complexes against chloroquine-sensitive and resistant strains of the *Plasmodium falciparum* malaria parasite. *J. Inorg. Biochem.* **2019**, *191*, 164–173.

(32) Rajapakse, C. S. K.; Martínez, A.; Naoulou, B.; Jarzecki, A. A.; Suárez, L.; Deregnacourt, C.; Sinou, V.; Schrével, J.; Musi, E.; Ambrosini, G.; Schwartz, G. K.; Sánchez-Delgado, R. A. Synthesis, Characterization and in vitro Antimalarial and Antitumor Activity of New Ruthenium(II) Complexes of Chloroquine. *Inorg. Chem.* **2009**, *48*, 1122–1131.

(33) Martínez, A.; Rajapakse, C. S. K.; Jalloh, D.; Dautriche, C.; Sánchez-Delgado, R. A. The antimalarial activity of Ru-chloroquine complexes against resistant *Plasmodium falciparum* is related to lipophilicity, basicity, and heme aggregation inhibition ability near water/n-octanol interfaces. *JBIC, J. Biol. Inorg. Chem.* **2009**, *14*, 863–871.

(34) Nkoana, W.; Nyoni, D.; Chellan, P.; Stringer, T.; Taylor, D.; Smith, P. J.; Hutton, A. T.; Smith, G. S. Heterometallic half-sandwich complexes containing a ferrocenyl motif: Synthesis, molecular structure, electrochemistry and antiplasmodial evaluation. *J. Organomet. Chem.* **2014**, *752*, 67–75.

(35) Ekengard, E.; Glans, L.; Cassells, I.; Fogeron, T.; Govender, P.; Stringer, T.; Chellan, P.; Lisensky, G. C.; Hersh, W. H.; Doverbratt, I.; Lidin, S.; de Kock, C.; Smith, P. J.; Smith, G. S.; Nordlander, E. Antimalarial activity of ruthenium(II) and osmium(II) arene complexes with mono- and bidentate chloroquine analogue ligands. *Dalton Trans.* **2015**, *44*, 19314–19329.

(36) Rylands, L.-I.; Welsh, A.; Maepa, K.; Stringer, T.; Taylor, D.; Chibale, K.; Smith, G. S. Structure-activity relationship studies of antiplasmodial cyclometallated ruthenium(II), rhodium(III) and iridium(III) complexes of 2-phenylbenzimidazoles. *Eur. J. Med. Chem.* **2019**, *161*, 11–21.

(37) Adams, M.; de Kock, C.; Smith, P. J.; Land, K. M.; Liu, N.; Hopper, M.; Hsiao, A.; Burgoyne, A. R.; Stringer, T.; Meyer, M.; Wiesner, L.; Chibale, K.; Smith, G. S. Improved antiparasitic activity by incorporation of organosilane entities into half-sandwich ruthenium(II) and rhodium(III) thiosemicarbazone complexes. *Dalton Trans.* **2015**, *44*, 2456–2468.

(38) Adams, M.; Li, Y.; Khot, H.; De Kock, C.; Smith, P. J.; Land, K.; Chibale, K.; Smith, G. S. The synthesis and antiparasitic activity of arylid ferrocenyl-derived thiosemicarbazone ruthenium(II)–arene complexes. *Dalton Trans.* **2013**, *42*, 4677–4685.

(39) Macedo, T. S.; Colina-Vegas, L.; da Paixão, M.; Navarro, M.; Barreto, B. C.; Oliveira, P. C. M.; Macambira, S. G.; Machado, M.; Prudêncio, M.; D'Alessandro, S.; Basilico, N.; Moreira, D. R. M.; Batista, A. A.; Soares, M. B. P. Chloroquine-containing organo-ruthenium complexes are fast-acting multistage antimalarial agents. *Parasitology* **2016**, *143*, 1543–1556.

(40) Compound **Ru1**: Côte-Real, L.; Robalo, M. P.; Marques, F.; Nogueira, G.; Avecilla, F.; J. L. Silva, T.; C. Santos, F.; Tomaz, A. I.; Garcia, M. H.; Valente, A. The key role of coligands in novel ruthenium(II)-cyclopentadienyl bipyridine derivatives: Ranging from non-cytotoxic to highly cytotoxic compounds. *J. Inorg. Biochem.* **2015**, *150*, 148–159.

(41) Compounds **Ru1** and **Ru2**: Florindo, P. R.; Pereira, D. M.; Borralho, P. M.; Costa, P. J.; Piedade, M. F. M.; Rodrigues, C. M. P.; Fernandes, A. C. New $[(\eta^5\text{-C}_5\text{H}_5)\text{Ru}(\text{N}-\text{N})(\text{PPh}_3)]_2[\text{PF}_6]_2$ compounds: colon anticancer activity and GLUT-mediated cellular uptake of carbohydrate-appended complexes. *Dalton Trans.* **2016**, *45*, 11926–11930.

(42) Compound **Ru2** was first synthesized in 1987: Albers, M. O.; Liles, D. C.; Robinson, D. J.; Singleton, E. The chemistry of Cyclopentadienyl-Ruthenium and -Osmium Complexes. 5. The systematic synthesis of novel bridged diruthenium cations containing cyclopentadienyl and bidentate amine ligands. The crystal and molecular structure of $[\{(\eta^5\text{-C}_5\text{H}_5)\text{Ru}(\text{I},10\text{-phen})\}_2(\mu\text{-dppm})]$ -

$(\text{PF}_6)_2\cdot\text{CH}_2\text{Cl}_2$] [dppm = bis(diphenylphosphino)methane; phen = phenanthroline]. *Organometallics* **1987**, *6*, 2179–2189.

(43) Morais, T. S.; Valente, A.; Tomaz, A. I.; Marques, F.; Garcia, M. H. Tracking antitumor metallo-drugs: promising agents with the Ru(II)- and Fe(II)-cyclopentadienyl scaffolds. *Future Med. Chem.* **2016**, *8*, 527–544.

(44) Perrin, D. D.; Amarego, W. L. F.; Perrin, D. R. *Purification of Laboratory Chemicals*, 2nd ed.; Pergamon: New York, 1980.

(45) SABADS. *Area-detector Absorption Correction*; Bruker AXS Inc.: Madison, WI, 2004.

(46) SAINT, *Area-detector Integration Software*, ver. 7.23; Bruker AXS Inc.: Madison, WI, 2004.

(47) Sheldrick, G. M. A Short History of SHELX. *Acta Crystallogr., Sect. A: Found. Crystallogr.* **2008**, *64*, 112–122.

(48) Farrugia, L. J. WinGX and ORTEP for Windows: an update. *J. Appl. Crystallogr.* **2012**, *45*, 849–854.

(49) Macrae, C. F.; Edgington, P. R.; McCabe, P.; Pidcock, E.; Shields, G. P.; Taylor, R.; Towler, M.; van de Streek, J. Mercury: visualization and analysis of crystal structures. *J. Appl. Crystallogr.* **2006**, *39*, 453–457.

(50) Nogueira, F.; Diez, A.; Radfar, A.; Pérez-Benavente, S.; do Rosario, V. E.; Puyet, A.; Bautista, J. M. Early transcriptional response to chloroquine of the *Plasmodium falciparum* antioxidant defence in sensitive and resistant clones. *Acta Trop.* **2010**, *114*, 109–115.

(51) Aguiar, L.; Biosca, A.; Lantero, E.; Gut, J.; Vale, N.; Rosenthal, P. J.; Nogueira, F.; Andreu, D.; Fernández-Busquets, X.; Gomes, P. Coupling the Antimalarial Cell Penetrating Peptide TP10 to Classical Antimalarial Drugs Primaquine and Chloroquine Produces Strongly Hemolytic Conjugates. *Molecules* **2019**, *24*, 4559.

(52) Wilson, D. W.; Crabb, B. S.; Beeson, J. G. Development of fluorescent *Plasmodium falciparum* for in vitro growth inhibition assays. *Malar. J.* **2010**, *9*, 152.

(53) Fu, Y.; Tilley, L.; Kenny, S.; Klonis, N. Dual labeling with a far-red probe permits analysis of growth and oxidative stress in *P. falciparum*-infected erythrocytes. *Cytometry, Part A* **2010**, *77*, 253–263.

(54) Model, M. A.; Reese, J. L.; Fraizer, G. C. Measurement of wheat germ agglutinin binding with a fluorescence microscope. *Cytometry, Part A* **2009**, *75*, 874–881.

(55) Carvalho, C. M. L.; Chew, E.; Hashemy, S. I.; Lu, J.; Holmgren, A. Inhibition of the Human Thioredoxin System: a Molecular Mechanism of Mercury Toxicity. *J. Biol. Chem.* **2008**, *283*, 11913–11923.

(56) Prudêncio, M.; Mota, M. M.; Mendes, A. M. A toolbox to study liver stage malaria. *Trends Parasitol.* **2011**, *27*, 565–574.

(57) Ploemen, I. H. J.; Prudencio, M.; Douradinha, B. G.; Ramesar, J.; Fonager, J.; van Gemert, G.-J.; Luty, A. J. F.; Hermsen, C. C.; Sauerwein, R. W.; Baptista, F. G.; Mota, M. M.; Waters, A. P.; Que, I.; Lowik, C. W. G. M.; Khan, S. M.; Janse, C. J.; Franke-Fayard, B. M. D. Visualisation and Quantitative Analysis of the Rodent Malaria Liver Stage by Real Time Imaging. *PLoS One* **2009**, *4*, e7881.

(58) Groom, C. R.; Bruno, I. J.; Lightfoot, M. P.; Ward, S. C. The Cambridge Structural Database. *Acta Crystallogr., Sect. B: Struct. Sci., Cryst. Eng. Mater.* **2016**, *B72*, 171–179.

(59) Martínez, A.; Deregnacourt, C.; Sinou, V.; Latour, C.; Roy, D.; Schrével, J.; Sánchez-Delgado, R. A. Synthesis of an organo-ruthenium aminoquinoline-trioxane hybrid and evaluation of its activity against *Plasmodium falciparum* and its toxicity toward normal mammalian cells. *Med. Chem. Res.* **2017**, *26*, 473–483.

(60) PCC values range from 1 to –1, with 1 corresponding to a perfect correlation of the two images and –1 to uncorrelation: Dunn, K. W.; Kamocka, M. M.; McDonald, J. H. A practical guide to evaluating colocalization in biological microscopy. *Am. J. Physiol.* **2011**, *300*, C723–C742.

(61) Although **Ru4** and **Ru5** nuclear co-localization (confocal microscopy studies) is consistent with parasitic nuclear damage induced by **Ru2**, fluorophores are known to redirect compounds to different cellular organelles: Puckett, C. A.; Barton, J. K. Fluorescein Redirects a Ruthenium–Octarginine Conjugate to the Nucleus. *J.*

Am. Chem. Soc. **2009**, *131*, 8738–8739. Conclusions about the cellular distribution of compounds **Ru1–Ru3** would require parasitic cellular fractionation and analysis by ICP-MS or AAS.

(62) Rodrigues, C. A. B.; Frade, R. F. M.; Albuquerque, I. S.; Perry, M. J.; Gut, J.; Machado, M.; Rosenthal, P. J.; Prudêncio, M.; Afonso, C. A. M.; Moreira, R. Targeting the Erythrocytic and Liver Stages of Malaria Parasites with s-Triazine-Based Hybrids. *ChemMedChem* **2015**, *10*, 883–890.

(63) Derbyshire, E. R.; Prudêncio, M.; Mota, M. M.; Clardy, J. Liver-stage malaria parasites vulnerable to diverse chemical scaffolds. *Proc. Natl. Acad. Sci. U. S. A.* **2012**, *109*, 8511–8516.

(64) Camarda, G.; Jirawatcharadech, P.; Priestley, R. S.; Saif, A.; March, S.; Wong, M. H. L.; Leung, S.; Miller, A. B.; Baker, D. A.; Alano, P.; Paine, M. J. I.; Bhatia, S. N.; O'Neill, P. M.; Ward, S. A.; Biagini, G. A. Antimalarial activity of primaquine operates via a two-step biochemical relay. *Nat. Commun.* **2019**, *10*, 3226.